Density Functional Study of the Reppe Carbonylation of Acetylene

F. De Angelis and A. Sgamellotti*

Dipartimento di Chimica e Centro Studi CNR per il Calcolo Intensivo in Scienze Molecolari, Università di Perugia, I-06123 Perugia, Italy

N. Re

Facoltà di Farmacia, Università G. D'Annunzio, I-06100 Chieti, Italy

Received March 20, 2000

The Reppe carbonylation of acetylene has been investigated by both static and dynamic density functional methods. Structures of all intermediates and transition states involved in each step of the catalytic cycle have been determined using gradient-corrected exchange−correlation potentials. Dynamic simulations have been performed on the migrative insertion of CO into the metal−vinyl bond after CO coordination by the metal and show that the insertion is preceded by a Berry pseudorotation of the initial pentacoordinated reagent and occurs via a simultaneous detachment of the vinyl group from the metal and formation of the vinyl−carbonyl bond. The overall thermodynamics and kinetics for the full catalytic cycle have been evaluated and have shown that the Reppe carbonylation of acetylene is a thermodynamically favored and kinetically easy process.

1. Introduction

The Reppe carbonylation consists of the carbonylation of alkenes and alkynes using iron, cobalt, or nickel carbonyls as catalyst in the presence of a haloid acid.[1] In particular, the carbonylation of acetylene to acrylic ester on nickel carbonyl has been extensively studied due to its industrial importance.[2] The proposed catalytic cycle involves five steps: (a) the oxidative addition of HX to nickel carbonyl, (b) the addition of acetylene to the metal and its subsequent insertion into the Ni−H bond, (c′) the migrative insertion of CO into the Ni−$CH{=}CH_2$ bond followed by the coordination of a further CO molecule or (c″) the coordination of CO to nickel followed by the CO insertion into the nickel vinyl bond, and (d) the addition of a water molecule, with the elimination of acrylic acid; see Scheme 1.

Although the insertion of carbonyl into a metal−alkyl bond has already been studied,[3] no accurate calculation has been performed yet on the carbonyl insertion into a metal−alkenyl system.

A preliminary study of step (c′), by means of both static and dynamic density functional methods, using the Car−Parrinello approach,[4] have been already reported in a previous paper.[5]

In this work we will focus on the remaining steps involved in the whole catalytic cycle by a gradient-corrected density functional approach and extend our dynamics simulations to the different pathway c″ for migrative insertion. In particular, we will consider (a) the preliminary addition of HCl to nickel carbonyl,

Scheme 1

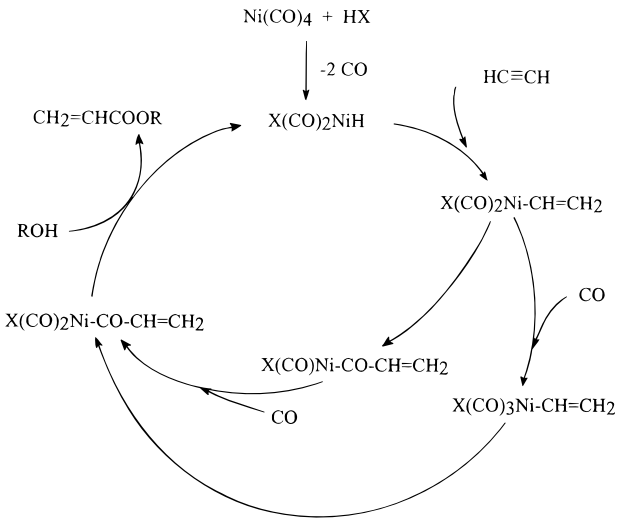

$$Ni(CO)_4 + HCl \rightarrow Cl(CO)_2NiH + 2CO$$

(b) the addition of acetylene to nickel,

$$Cl(CO)_2NiH + HC{\equiv}CH \rightarrow Cl(CO)_2NiH(HC{\equiv}CH)$$

and its subsequent insertion into the Ni−H bond,

$$Cl(CO)_2NiH(HC{\equiv}CH) \rightarrow Cl(CO)_2Ni{-}CH{=}CH_2$$

(c′) the migrative insertion of CO into the nickel−vinyl bond,

(1) Powell, P. *Principles of Organometallic Chemistry*; Chapman & Hall, London, 1988.
(2) Cornils, B.; Herrmann, W. A. *Applied Homogeneous Catalysis with Organometallic Compounds*; VCH: Weinheim, 1996.
(3) Matsubara, T.; Koga, N.; Ding, Y.; Musaev, D. G.; Morokuma, K. *Organometallics* **1997**, *16*, 1065−1078. Koga, N.; Morokuma, K. *New J. Chem.* **1991**, *15*, 749. Koga, N.; Morokuma, K. *J. Am. Chem. Soc.* **1986**, *108*, 6136.
(4) Car, R.; Parrinello, M. *Phys. Rev. Lett.* **1985**, *55*, 2471.
(5) De Angelis, F.; Re, N.; Sgamellotti, A.; Selloni, A.; Weber J.; Floriani, C. *Chem. Phys. Lett.* **1998**, *291*, 57.

10.1021/om0002428 CCC: $19.00
Publication on Web 08/31/2000

$$Cl(CO)_2Ni{-}CH{=}CH_2 \rightarrow Cl(CO)Ni{-}CO{-}CH{=}CH_2$$

followed by addition of CO to the nickel η^1 acyl complex,

$$Cl(CO)Ni{-}CO{-}CH{=}CH_2 + CO \rightarrow Cl(CO)_2Ni{-}CO{-}CH{=}CH_2$$

or (c″) the coordination of CO to $Cl(CO)_2Ni{-}CH{=}CH_2$,

$$Cl(CO)_2Ni{-}CH{=}CH_2 + CO \rightarrow Cl(CO)_3Ni{-}CH{=}CH_2$$

followed by the migrative insertion of CO into the nickel−vinyl bond,

$$Cl(CO)_3Ni{-}CH{=}CH_2 \rightarrow Cl(CO)_2Ni{-}CO{-}CH{=}CH_2$$

(d) the attack of a water molecule followed by the elimination of acrylic acid,

$$Cl(CO)_2Ni{-}CO{-}CH{=}CH_2 + H_2O \rightarrow Cl(CO)_2NiH + CH_2{=}CHCOOH$$

For each of the considered elementary steps we have identified the equilibrium geometries and the relative energies of stable configuration for all the involved molecules and evaluated the overall reaction energies. For steps b, c′, and c″ we computed the corresponding transition states, and for step c″ we performed also dynamic simulations, to gain further insight into the reaction mechanism of the migrative insertion reaction. We have finally evaluated the overall thermodynamics and kinetics for the full catalytic cycle.

2. Computational Details

Static DFT Calculations. The static DFT calculations reported in this paper have been performed using the Gaussian 94 program package.[6] We used a 6-311G** basis set[7] for chlorine, carbon, and hydrogen atoms; the Ni basis set is a [8s4p3d] contraction[8] of the primitive set of Wachters.[9]

Geometry optimizations were performed on all the stationary points of the potential energy surface for steps a, b, c′, c″, and d both in cis and trans coordination with the Vosko−Wilk−Nusair LDA parametrization[10] and including the Becke[11] and Perdew−Wang[12] gradient corrections (GC) to the exchange and correlation, respectively. For steps a, b, and c″ we also computed the geometries of the different stable pentacoordinated Ni−acetylene complexes. The transition states were obtained by the synchronous transit-guided quasi-Newton method available in Gaussian 94.[13] All stationary points were optimized without any symmetry constraints, and transition states were checked by computing the vibrational frequencies.

The reaction pathway for acetylene insertion was traced by the intrinsic reaction coordinate (IRC) method based on a search scheme by Schlegel et al.[14,15] and implemented in Gaussian.

Car−Parrinello Calculations. Molecular dynamics simulations were carried out with the Car−Parrinello (CP) method[4] for step c″. Gradient-corrected calculations have been performed using our parallel version of the CP code.[16] For the LDA exchange−correlation functional the Perdew−Zunger parametrization[17] has been used, while the gradient-corrected functional is taken from ref 18. Core states are projected out using pseudopotentials. For Ni, C, and O "ultrasoft" pseudopotentials were generated according to the scheme proposed by Vanderbilt,[19] whereas for Cl the Bachelet−Hamann−Schluter (BHS) pseudopotential[20] has been used. The wave functions were expanded in plane waves up to an energy cutoff of 25 Ry. Periodic boundary conditions were used by placing the model molecule in a cubic box of 10.6 Å, sufficiently large to avoid coupling between periodic images. The equations of motion were integrated using a time step of 6 au (0.145 fs) with an electronic fictitious mass $\mu = 2000$ au.

3. Results and Discussion

The initial key step of the Reppe carbonylation is the oxidative addition of chloridric acid to nickel tetracarbonyl (step a), leading to the catalytically active species $Cl(CO)_2NiH$,

$$Ni(CO)_4 + HCl \rightarrow Cl(CO)_2NiH + 2CO$$

The geometry of $Ni(CO)_4$, **1a**, was optimized leading to a tetrahedral structure with $R(Ni{-}C) = 1.804$ Å and $R(C{-}O) = 1.151$ Å, in good agreement with the experimental geometry ($R(Ni{-}C) = 1.825$ Å and $R(C{-}O) = 1.122$ Å).

We first investigated the energetics of CO loss from $Ni(CO)_4$, considering both the loss of one CO molecule, leading to $Ni(CO)_3$, **1b**, and the simultaneous detachment of two CO molecules, leading to $Ni(CO)_2$, **1c**. We found the first process (loss of one CO) to be endothermic by 114 kJ mol^{-1}, while the simultaneous loss of two CO molecules was found endothermic by 311 kJ mol^{-1}. To check the existence of an activation barrier to the loss of one CO from $Ni(CO)_4$, we performed a linear transit scan of the potential energy surface, by constraining the Ni−CO distance at fixed values in the range 1.85−4.00 Å and optimizing all the other geometrical parameters; no energy barrier was found for the detachment of the CO molecule.

We then optimized the geometry of all the possible pentacoordinated trigonal-bipyramidal (TBP) isomers of the $Cl(CO)_3$ NiH complex, resulting from HCl addition to $Ni(CO)_3$. We found the isomer with axial Cl and H, **1d**, to be fairly the most stable, though with a formation energy of +41 kJ mol^{-1}. Stability of different TBP isomers will be addressed in the next section of this paper. The further loss of a CO molecule from **1d** leads to the formation of the catalytically active $Cl(CO)_2NiH$ complex **2**, with an endothermicity of 58 kJ mol^{-1}. In this case also, a linear transit scan of the potential energy surface corresponding to the loss of a CO

(6) Frisch, M. J.; Trucks, G. W.; Schlegel, H. M.; Gill, P. M. W.; Johnson, B. G.; Wong, M. W.; Foresman, J. B.; Robb, M. A.; Head-Gordon, M.; Replogle, E. S.; Gomperts, R.; Andres, J. L.; Raghavachari, K.; Binkley, J. S.; Gonzales, C.; Martin, R. L.; Fox, D. J.; Defrees, D. J.; Baker, J.; Stewart, J. J. P.; Pople, J. A. *Gaussian 94* (Revision A.1); Gaussian Inc.: Pittsburgh, PA, 1994.
(7) Frisch, M. J.; Pople J. A.; Binkley, J. S. *J. Chem. Phys.* **1984**, *80*, 3265, and references therein.
(8) Hay, P. J. *J. Chem. Phys.* **1977**, *77*, 4377.
(9) Wachters, A. J. H. *J. Chem. Phys.* **1970**, *52*, 1033.
(10) Vosko, S. H.; Wilk, L.; Nusair, M. *Can. J. Phys.* **1980**, *58*, 1200.
(11) Becke, A. D. *Phys. Rev.* **1988**, *A38*, 3098.
(12) Perdew, J. P.; Wang, Y. *Phys. Rev.* **1992**, *B45*, 13244.
(13) Simons, J.; Jorgensen, P.; Taylor H.; Ozment, J. *J. Phys. Chem.* **1983**, *87*, 2745.
(14) Gonzalez, C.; Schlegel, H. B. *J. Chem. Phys.* **1989**, *90*, 2154.
(15) Gonzalez, C.; Schlegel, H. B. *J. Phys. Chem.* **1990**, *94*, 5523.
(16) The implementation that we use is decribed in: Pasquarello, A.; Laasonen, K.; Car, R.; Lee, C.; Vanderbilt, D. *Phys. Rev. Lett.* **1992**, *69*, 1982; Pasquarello, A.; Laasonen, K.; Car, R.; Lee, C.; Vanderbilt, D. *Phys. Rev. B* **1993**, *47*, 10142.
(17) Perdew, J. P.; Zunger, A. *Phys. Rev. B* **1981**, *23*, 5048.
(18) Perdew, J. P.; Chevary, J. A.; Vosko, S. H.; Jackson, K. A.; Pederson, M. R.; Singh, D. J.; Fiolhais, C. *Phys. Rev. B* **1992**, *46*, 6671.
(19) Vanderbilt, D. *Phys. Rev. B* **1990**, *41*, 7892.
(20) Bachelet, G. B.; Hamann, D. R.; Schlüter, M. *Phys. Rev. B* **1982**, *26*, 4199.

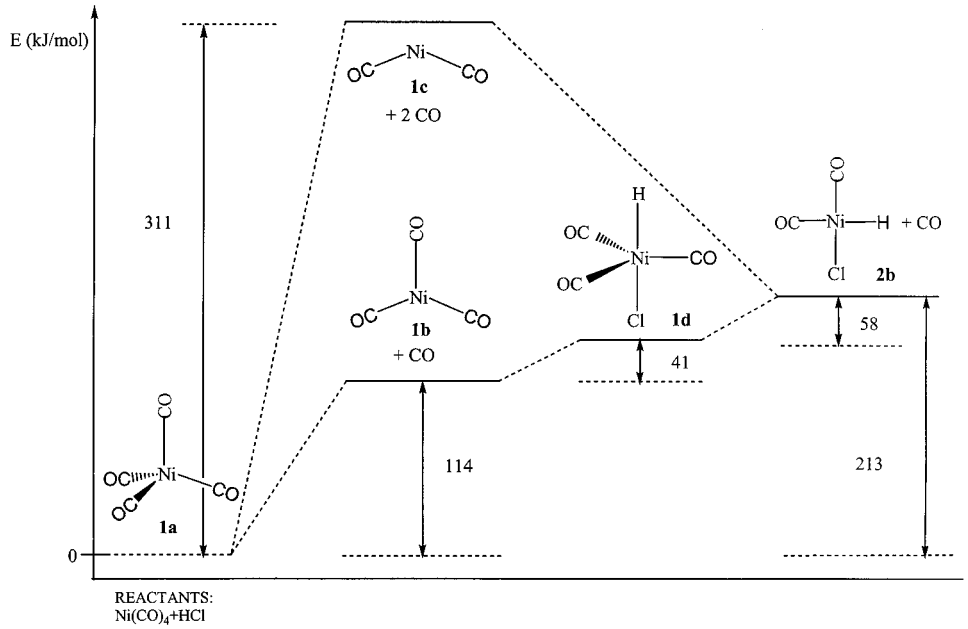

Figure 1. Schematic representation of the potential energy surface for step a.

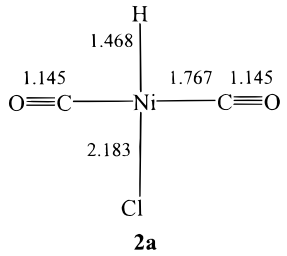

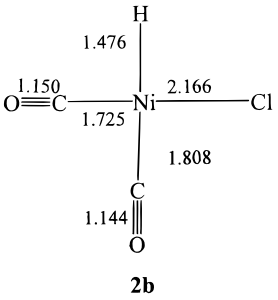

Figure 2. Main geometrical parameters of catalyst **2** in trans (**2a**) and cis (**2b**) coordination. Distances in Å.

molecule has been performed and shows that no activation barrier exists for the loss of a CO molecule from **1d**.

The best pathway for the formation of the catalytically active species **2** seems therefore the loss of a CO molecule by $Ni(CO)_4$, followed by the addition of the HCl molecule and then the detachment of a second CO molecule; see Figure 1.

A full geometry optimization of **2** led to a nearly square-planar cis structure, with the trans isomer 8.3 kJ mol^{-1} higher in energy. The optimized structures are shown in Figure 2 together with the main geometrical parameters. The greater stability of the cis isomer is a general trend we found in most of the considered square-planar dicarbonyl complexes and is probably due to the mutual trans destabilization of two carbonyl groups. The only exception is the tetracoordinated species of step c, for which the trans isomer was found slightly more stable than the cis one, although by a negligibly small energy, about 2 kJ mol^{-1} (see below).

The overall reaction was found quite endothermic, 213 kJ mol^{-1}, as expected on the basis of the high metal−carbonyl dissociation energies. This value can be regarded as an overestimate of the real reaction energy, since our calculations did not account either for the stabilization of **2** by solvent coordination or for the possibility that the process takes place in concert with the strongly exothermic acetylene complexation and insertion (vide infra).

3.1. Acetylene Insertion. The first step of acetylene insertion involves the coordination of acetylene to **2**, yielding the pentacoordinated complex $Cl(CO)_2NiH(HC{\equiv}CH)$, **3**. There exist seven possible trigonal-bipyramidal (TBP) isomers of **3**; see Figure 3, which can be connected via Berry pseudorotations (BPR) through square-pyramidal transition states. Geometry optimizations performed under C_s and C_1 symmetry constraints have shown that only isomers **3a**−**c** have stable equilibrium structures. Isomers **3d**−**g**, having an equatorial hydride ligand, are not stable, rather constituting transition states between the other TBP structures.

Geometrical parameters for the three stable isomers **3a**−**c** are shown in Figure 4 together with the relative energies. We calculate as lowest isomer the TBP structure **3a** with H and Cl in axial positions, with **3b** (H and acetylene axial) 16 kJ mol^{-1} and **3c** (H and CO axial) 21 kJ mol^{-1} higher in energy.

Site preference for axial hydride and equatorial ethylene have been already observed for analogous d^8 pentacoordinated complexes involved in ethylene insertion processes.[21−23] This preference has been rationalized in terms of (i) the stronger σ bond formed by the axial hydride with the vacant d_{x^2} orbital and (ii) the better

(21) Mastubara, T.; Koga, N.; Dirg, Y.; Musaev, D. G.; Morokuma, K. *Organometallics* **1997**, *16*, 1065.
(22) Koga, N.; Jin, S. Q.; Morokuma, K. *J. Am. Chem. Soc.* **1988**, *110*, 3417
(23) Versluis, L.; Ziegler, T.; Fan, L. *Inorg. Chem.* **1990**, *29*, 4530.

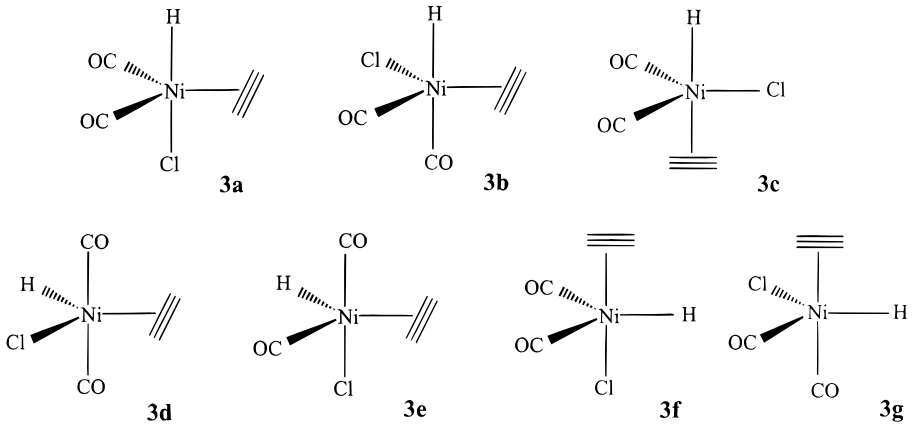

Figure 3. Geometrical structures of the seven possible pentacoordinated TBP isomers of **3**.

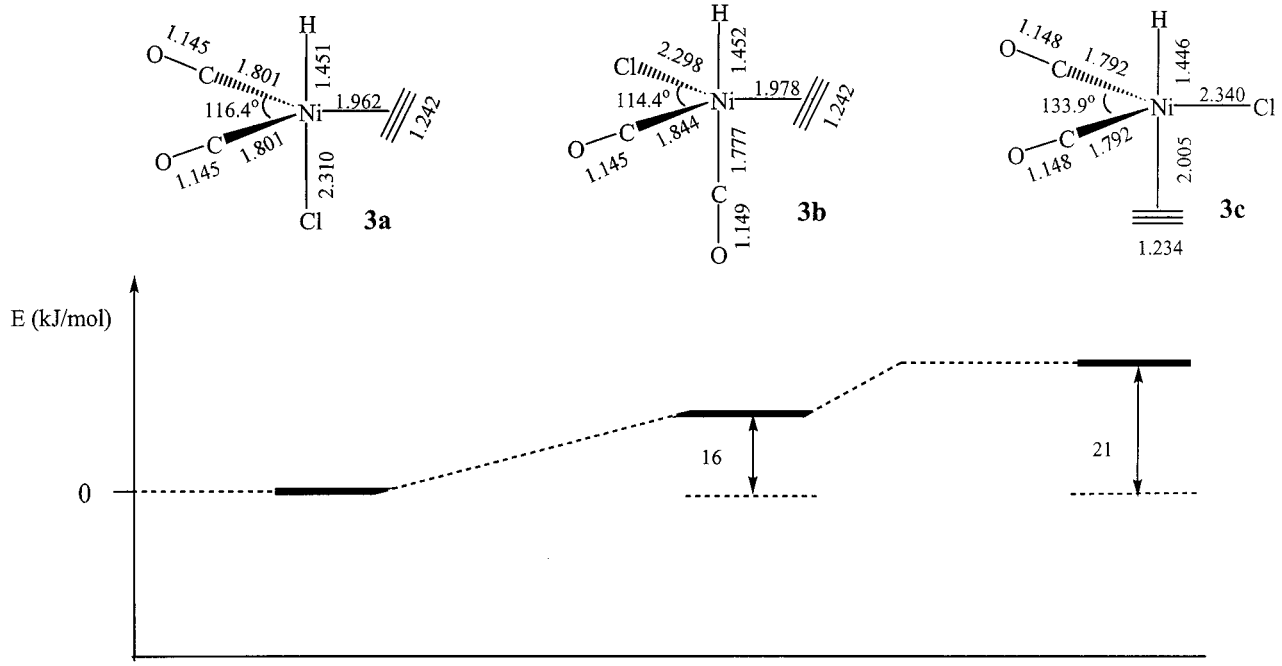

Figure 4. Main geometrical parameters and relative stabilities of TBP stable isomers **3a**−**c**. Distances in Å, angles in deg, and energies in kJ mol^{-1}.

back-donation from the occupied $d_{x^2-y^2}$ and d_{xy} orbitals in the equatorial plane to the π^* orbitals of ethylene. The same arguments apply to the acetylenic complex **3** and also explain the higher stability of the isomer **3a**, which presents the two σ-donor ligands, H and Cl, in axial position; see Figure 4.

The nickel−acetylene bonding energy has been calculated to be 21 kJ mol^{-1} in the most stable isomer, **3a**, a relatively small value as expected on the basis of the high stability of Ni d^8 square-planar coordination.

We have then addressed the intramolecular acetylene insertion in the TBP complex **3**. We considered only the two more stable isomers, **3a** and **3b**, since **3c** (with acetylene trans to the hydride ligand) has to rearrange to either one of the former isomers in order to bring acetylene close to the hydride prior to the insertion process. Two reaction paths for acetylene insertion can be conceived for both isomers **3a** and **3b**; see Figure 5. In the first path, the equatorial acetylene has to rotate around the Ni−C_2H_2 axis by about 90° to approach suitably the axial hydride with the C−C bond parallel to Ni−H. In the second path the TBP structure undergoes a BPR to a square-pyramidal geometry, and the reaction takes place between the basal acetylene and hydride.

We first considered the rotation of acetylene around the Ni−C_2H_2 axis in **3a**, finding a transition state for this conformational process, corresponding to a rotation of 90°, about 12 kJ mol^{-1} higher in energy. This geometry, hereafter referred to as **3a′**, corresponds to a stable structure in C_s geometry and has been considered as the starting point for the acetylene insertion. Hence we searched the transition state for the insertion reaction along this path, finding a structure 15 kJ mol^{-1} higher than **3a′** and therefore 27 kJ mol^{-1} above **3a**, which will hereafter be referred to as TS1.

We then searched for the transition state for the insertion reaction along an analogous path starting from the less stable isomer **3b**. We found a transition state, hereafter called TS2, 15 kJ mol^{-1} higher in energy than the corresponding reagent, i.e., isomer **3b**, thus 31 kJ mol^{-1} higher than isomer **3a** and 4 kJ mol^{-1} higher than TS1. The configuration of the reaction center of TS2 was found quite similar to that of TS1, with the hydrogen

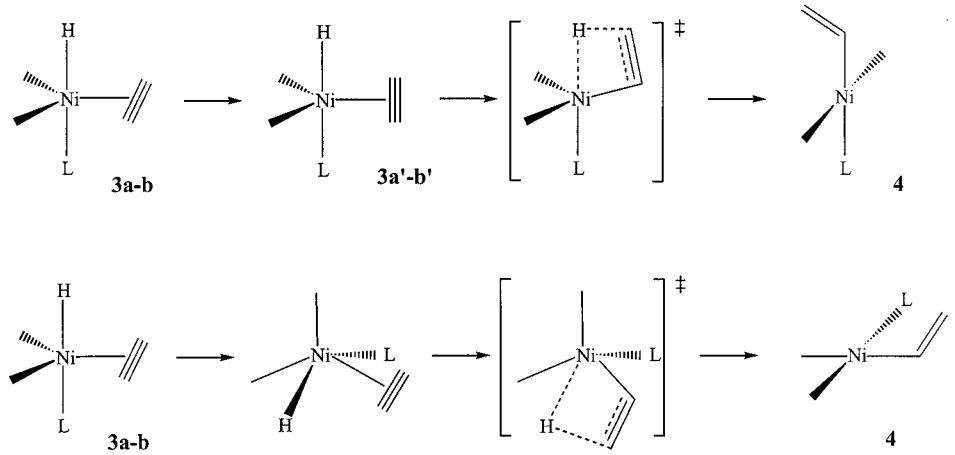

Figure 5. Possible pathways for acetylene insertion into the Ni−H bond, starting from **3**.

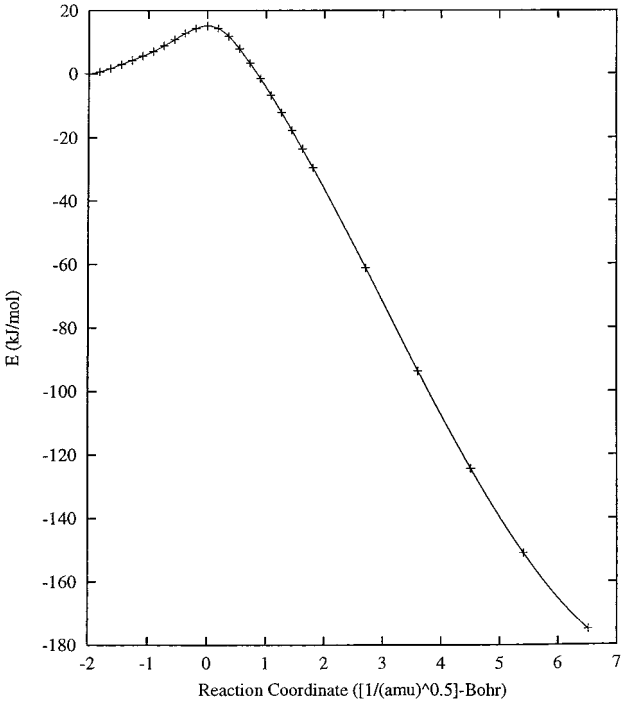

Figure 6. IRC energy profile as a function of the computed reaction coordinate for the acetylene insertion from **3a′** to **4**. Energy scale in kJ mol^{-1}.

bound to the metal center bent toward the inserting acetylene carbon, with a hydride−acetylene carbon distance of ca. 1.7 Å. We therefore limited our discussion to the lower lying transition state TS1, starting from **3a**, even though analogous considerations hold for TS2. The pathway of the insertion reaction from **3a′** to the final $Cl(CO)_2Ni{-}CH{=}CH_2$, **4**, was traced by the IRC method, and the calculated energy profile is shown in Figure 6. The reaction coordinate was found to be largely composed by the distance between the nickel-bound hydrogen and one of the two acetylene carbons (the β carbon of the forming vinyl group) and by the Ni−H−C angle; the coefficients related to other geometrical parameters are almost negligible, so that we can rationalize this step as a hydrogen transfer from the Ni atom to the HC≡CH fragment.

From the above discussion we might regard the insertion reaction as composed by two steps: (i) the rotation of HC≡CH around the Ni−acetylene bond and (ii) the subsequent migration of a hydrogen from Ni to the HC≡CH fragment. However, in the experimental conditions of the reaction (ca. 500 K), due to the low energy barrier the rotation around the Ni−acetylene bond should be almost free, so that the two steps cannot be clearly distinguished.

We also searched for the transition states corresponding to the second path of Figure 5, in which **3a** and **3b** undergo a BPR to a square-pyramidal geometry, and the insertion takes place between the basal acetylene and hydride. However, no square-pyramidal intermediate nor transition state could be found for this path.

From the IRC energy profile in Figure 6, we can see how the path leading to the product is much steeper than the one leading to the reagent, so that we may think this reaction step to be easily driven toward the product both by the low energy barrier and by the high exothermicity of the reaction itself.

The overall insertion reaction $Cl(CO)_2NiH + HC{\equiv}CH \rightarrow Cl(CO)_2Ni{-}CH{=}CH_2$ was found to be highly exothermic, $\Delta E = -189$ kJ mol^{-1} with a small activation barrier of 27 kJ mol^{-1}. It is worth noting that high exothermicity (−132 kJ mol^{-1}) and a low energy barrier (3 kJ mol^{-1}) were found also for ethylene insertion into the Ni−H bond of $Ni(PH_3)(H_2)$ at the MP2 level.[26] To the best of our knowledge, a comparison of thermodynamical and kinetical data between acetylene and ethylene insertion into the metal−hydrogen bond has been performed only on square-planar Pd complexes[25] and showed that acetylene insertion is much more exothermic, but it has to overcome a higher energy barrier.

3.2. CO Insertion. Two different pathways may be conceived for the migrative insertion of CO into the nickel−vinyl bond and the subsequent formation of a tetracoordinated acyl complex: (i) the migrative insertion takes place directly from the tetracoordinated complex $Cl(CO)_2Ni{-}CH{=}CH_2$, leading to tricoordinated acyl complex, which is finally coordinated by an external CO molecule; (ii) an external CO molecule is first coordinated to $Cl(CO)_2Ni{-}CH{=}CH_2$, leading to a pen-

(24) Atwood, J. D. *Inorganic and Organometallic Reaction Mechanism*; Wadsworth Inc.: Belmont CA, 1985, Vol. 136, and references therein.
(25) de Vaal, P.; Dedien, A. *J. Organomet. Chem.* **1994**, *478*, 121.
(26) Koga, N.; Obara, L.; Kitoura, M.; Morokuma, K. *J. Am. Chem. Soc* **1985**, *107*, 7109.

Scheme 2

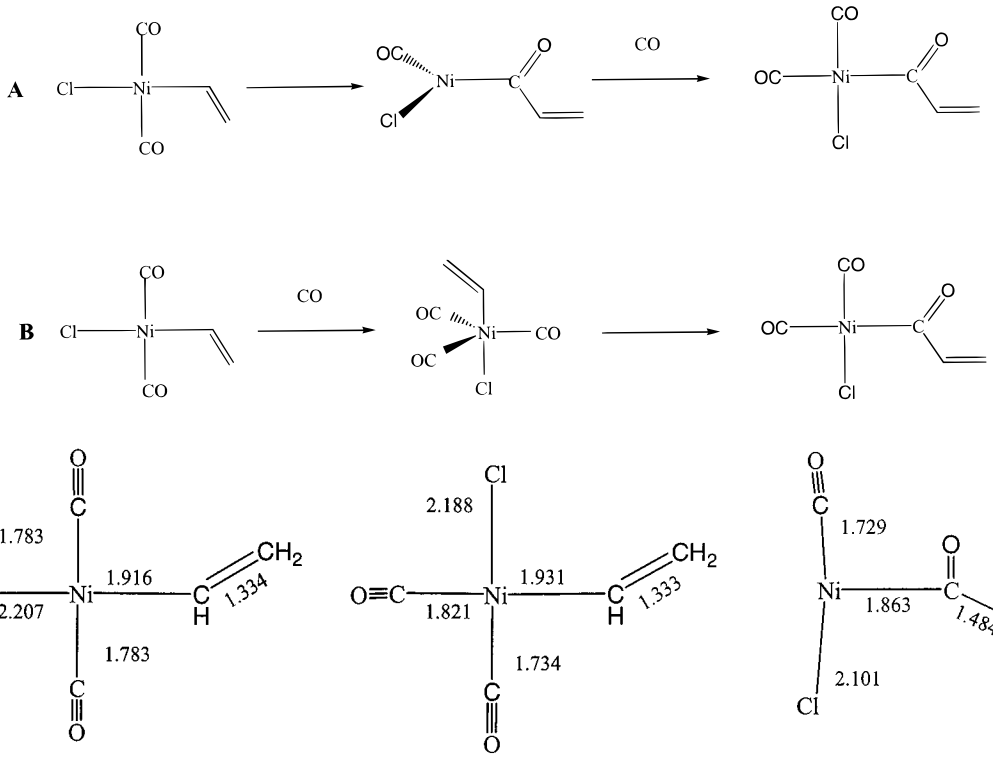

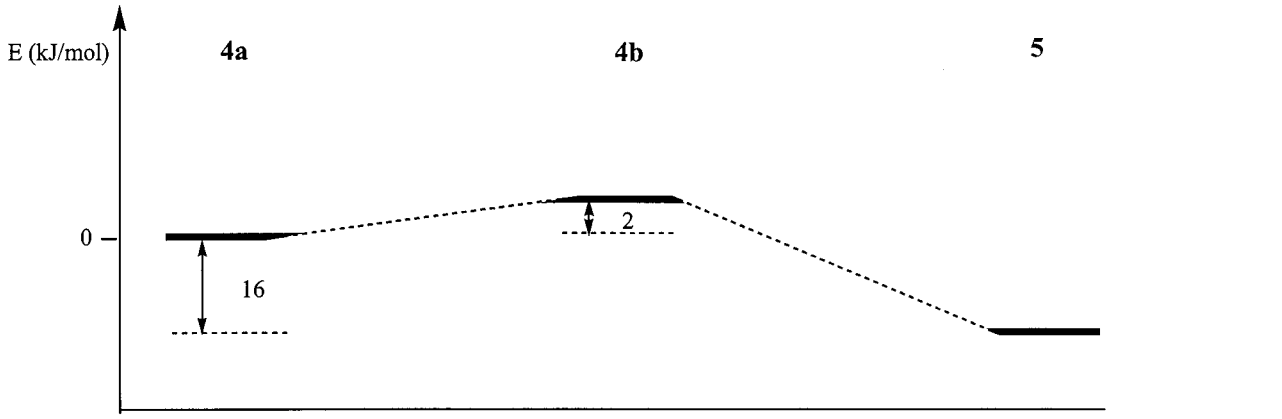

Figure 7. Main geometrical parameters and relative stabilities of complexes **4**, in trans (**4a**) and cis (**4b**) coordination, and of **5**. Distances in Å and energies in kJ mol^{-1}.

tacoordinated tricarbonyl complex, from which the carbonyl insertion takes place (A and B, respectively, in Scheme 2).

Migrative Insertion from 4. A full geometry optimization of the vinyl complex $Cl(CO)_2Ni-CH=CH_2$, **4**, led to a nearly square-planar trans structure **4a**; see Figure 7. The calculated structure reveals an almost planar arrangement of the four ligands with the vinyl plane perpendicular to the plane of coordination to reduce the steric interaction between the α hydrogen and the adjacent carbonyls. A second minimum corresponding to a nearly square-planar cis isomer, **4b**, has been found 2 kJ mol^{-1} higher in energy. Figure 7 shows also the optimized geometry of the $Cl(CO)Ni-COCH=CH_2$ product, **5**, corresponding to a trigonal geometry in a "T" configuration, with the $COCH=CH_2$ ligand trans to the vacant coordination site. We have calculated the transition state for the insertion reaction, finding a structure quite similar to that of the cis reagent **4b**, with the vinyl plane still essentially perpendicular to the ligand plane and the inserting carbonyl slightly bent toward the vinyl α carbon. Normal-mode analysis performed on the structure of the transition state has shown that the computed structure is properly correlated through the reaction mode to the **4b** isomer. For the sake of completeness we searched for the transition state for the migrative insertion starting from **4a**, finding a structure 40 kJ mol^{-1} higher in energy than **4a**, with an arrangement of the reaction center similar to that of the transition state correlating with **4b**. The reaction has been found slightly exothermic (−16 kJ mol^{-1}) with a low energy barrier (9 kJ mol^{-1}). It is interesting to compare the results for the energetics of the CO insertion into the nickel−vinyl bond with the experimental data for the CO insertion into some metal−alkyl bonds. The insertion reactions into the latter bonds have been found always slightly endothermic with correspondingly higher energy barriers,[24] e.g.,

Scheme 3

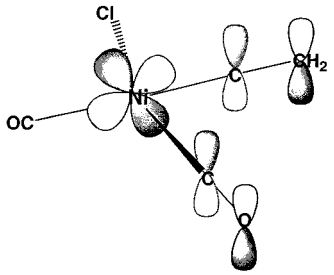

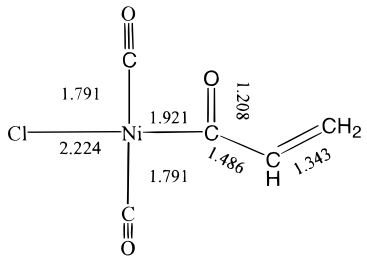

7a

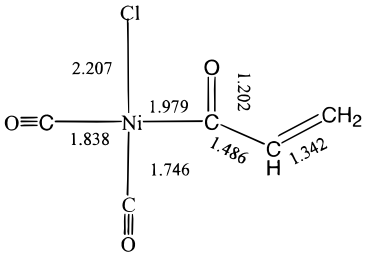

7b

Figure 8. Main geometrical parameters of **7** in cis (**7a**) and trans (**7b**) coordination. Distances in Å.

$\Delta H^{\ddagger} = 59$ kJ mol^{-1} for $(CO)_5MnMe$ and $\Delta H^{\ddagger} = 67$ kJ mol^{-1} for $PtI(Et)(CO)(PPh_3)$.

These results suggest therefore that the CO insertion in a metal−alkenyl bond is both thermodynamically and kinetically more favored than in a metal−alkyl bond. This difference can be attributed to the presence of the π system of the alkenyl ligand, which stabilizes both the product through conjugation with the carbonyl π orbital in the acyl moiety and the transition state through the extended π interaction shown in Scheme 3.

The coordinatevely unsaturated complex **5** is easily coordinated by an external CO molecule, leading to the tetracoordinated complex $Cl(CO)_2Ni-CO-CH=CH_2$, **7**. Geometry optimizations of this complex led to a nearly square-planar cis structure, **7a**, with the trans isomer, **7b**, 9.0 kJ mol^{-1} higher in energy. In both isomers the acyl plane was found still essentially perpendicular to the plane of coordination. The optimized geometries are shown in Figure 8 together with the geometrical parameters. The CO coordination was found quite exothermic with $\Delta E = 80$ kJ mol^{-1}. This is not surprising considering the greater stability of tetracoordinated 16-electron Ni complexes with respect to 14-electron tricoordinated ones.

Migrative Insertion after CO Coordination. We then considered the second path for the formation of **7**, in which an external CO molecule is first coordinated by **4**, leading to a pentacoordinated TBP complex, hereafter indicated as **6**. The carbonyl insertion might then take place from this species by direct attack of a CO group to the α carbon of the vinyl group, leading to the formation of **7**. To study this path, we first performed geometry optimizations of complex **6** on all four possible TBP isomers, i.e., **6a** with axial chlorine and vinyl groups, **6b** with axial vinyl and carbonyl, **6c** with axial chlorine and carbonyl, and **6d** with both carbonyls in axial position; see Figure 9. We found only isomers **6a**, **6b**, and **6c** to be stable minima of the C_s potential energy surface, while no stable minimum was found for the isomer **6d**. We computed isomer **6a** the more stable, with a coordination energy of 34 kJ mol^{-1}, while isomer **6b** was found 8 kJ mol^{-1} higher in energy. Isomer **6c** was found 75 kJ mol^{-1} higher in energy than **6a** and, therefore, not stable with respect to the free reagents. This is in agreement with the expected trend of stability of TBP isomers discussed above, always showing axial preference for σ-donor ligands.

We then performed a transition state search starting from complex **6a**, finding an energy barrier of 24 kJ mol^{-1} for the carbonyl insertion; the structure of this transition state was found quite close to that of complex **6a**, with the inserting carbonyl slightly bent toward the vinyl group. The insertion reaction from **6a** to **7** has been found quite exothermic (−60 kJ mol^{-1}); this value is well higher than the value found for the CO insertion from **4** to **5** (−16 kJ mol^{-1}, see above) probably because of the higher stability of the tetracoordinated acyl complex **7** with respect to the tricoordinated **5**. Due to the low energy difference between **6a** and **6b**, we computed also the transition state for CO insertion starting from complex **6b**. We found an energy barrier of 17 kJ mol^{-1} and a geometry of the reaction center almost identical to that of the TS obtained starting from **6a**. Thus both reaction pathways leading to **7** from isomers **6a** and **6b** are energetically accessible, although the latter requires a slightly higher energy barrier (25 vs 24 kJ mol^{-1}). A comparison between the two considered pathways for the CO insertion, A and B in Scheme 2, shows that the latter is energetically favored, since its transition state is 20 kJ mol^{-1} lower than the transition state of pathway A; see Figure 10. It is worth noting that the geometry of the reaction center calculated for the two transition states for the migrative insertion starting from **6a** and **6b** is quite similar to that found for the transition state starting from the tetracoordinated complex **4** (path A), suggesting that the potential energy surface for the migrative CO insertion is similar for both pathways. To gain further insight into the reaction mechanism for migrative CO insertion corresponding to pathway B, we performed molecular dynamics simulations starting from the more stable complex **6a**.

Dynamics Calculations. The dynamics of the CO insertion into the nickel−vinyl bond was simulated with the CP method at 600 K, using complex **6a** as a model reactant. We did not apply any constraints to the nuclear coordinates, allowing all the degrees of freedom to evolve naturally in time; however, we used a temperature slightly higher than the experimental employed one (ca. 500 K) to speed up the reaction. Because

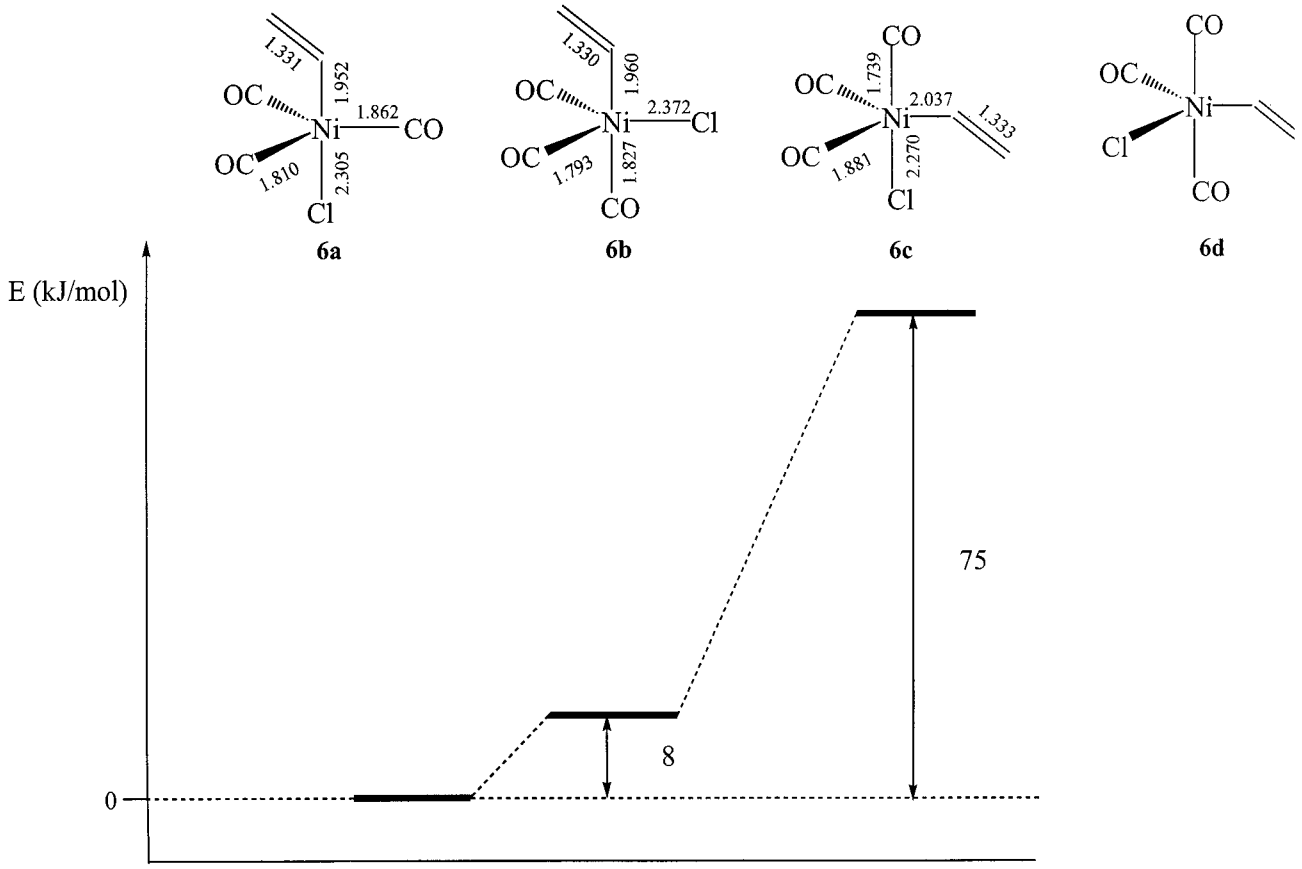

Figure 9. Geometrical structures and relative stabilities of the four possible TBP isomers of **6**. Distances in Å and energies in kJ mol^{-1}.

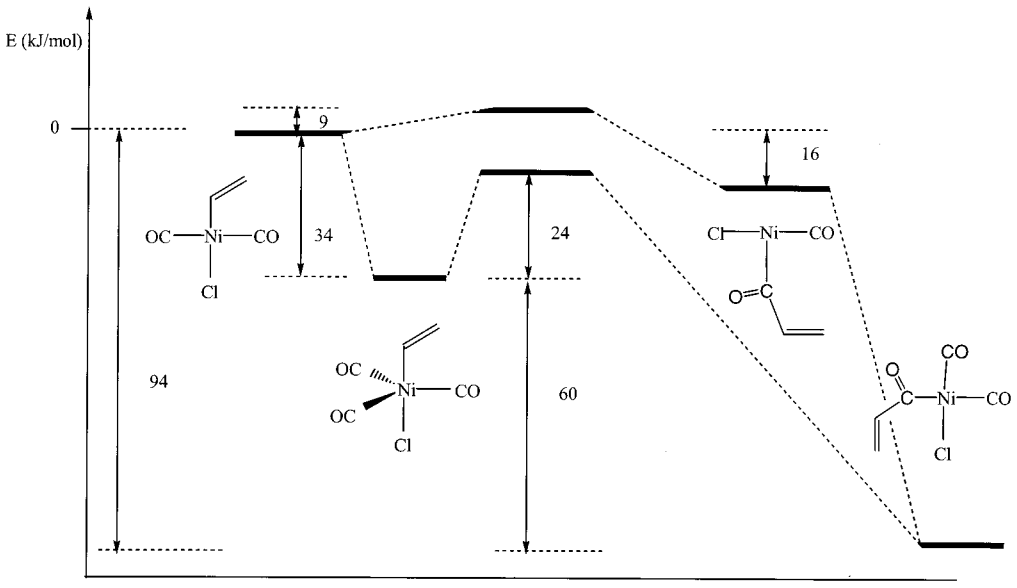

Figure 10. Schematic representation of the potential energy surfaces for the two possible pathways A and B for CO insertion. Energies in kJ mol^{-1}.

of the relatively high energy barrier (24 kJ mol^{-1}), the observation time was extended up to 7.5 ps.

To check the consistency between the CP approach and our static DFT calculations, we optimized the structure of **6a**, **6b**, and **7** with the CP method, finding very good agreement between the two approaches, with average differences of less than 0.008 Å and 0.5° on bond lengths and bond angles, respectively. Moreover, we computed the energy difference between **6a** and **6b** to be 6 kJ mol^{-1} and the exothermicity of the reaction leading to **7** to be −60 kJ mol^{-1}, in very good agreement with the values obtained from static calculations (8 and −60 kJ mol^{-1}).

We started the molecular dynamics simulation by heating the structure of the more stable isomer **6a** with the geometry found in the CP optimization. To obtain a thermal distribution of vibrational modes, the temperature was gradually increased (via rescaling of ionic

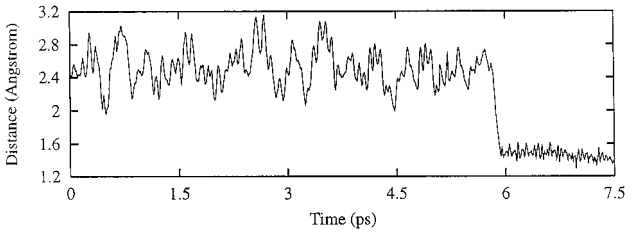

Figure 11. Time evolution of the C−C (carbonyl−vinyl) distance during the dynamics simulation. Time in ps and distance in Å.

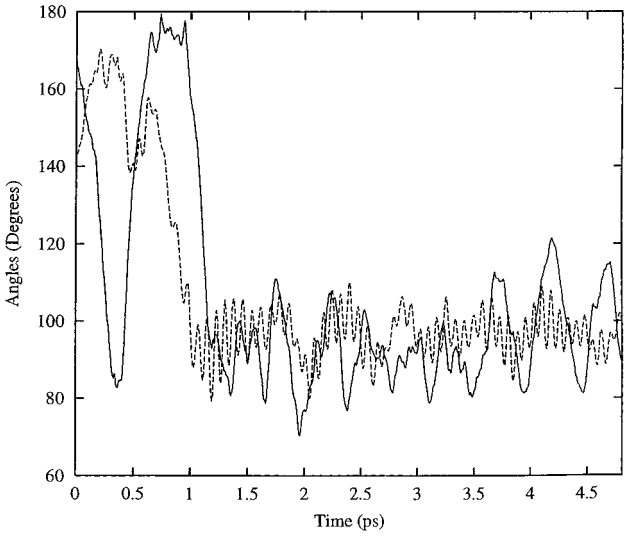

Figure 12. Time evolution of the Cl−Ni−C (chlorine−vinyl) (solid line) and C−Ni−C angle (carbonyl−carbonyl) (dashed line) for the first part of the dynamics simulation. Time in ps and angles in deg.

velocities) by small steps. The evolution of the CO insertion can be followed by studying the time evolution of the C−C distance between the carbonyl group and the metal attached carbon of the vinyl moiety. This C−C distance is 2.60 Å in the CP-optimized reagent structure **6a**, in which the two carbons are part of two different ligands, while it is only 1.48 Å in the product **7**, where the two carbons are directly bonded. Figure 11 displays the variation of this C−C distance as a function of the simulation time. From Figure 11 it appears that the reactive CO migration takes place within ca. 6 ps. Indeed, a fast decrease in the C−C distance from ca. 2.6 to ca. 1.5 Å is observed around 6 ps. Thereafter, the C−C distance varies within the normal limits of C−C vibration.

In the following discussion, we have divided the time span of the simulation into two portions, with the first one going up to ca. 4.5 ps, to discuss geometrical variations in more detail.

To check whether the TBP isomer **6b** plays some role in the migrative insertion reaction, we have analyzed the variation of the Cl−Ni−C (vinyl) bond angle, as a function of the simulation time (see Figure 12); this angle, indeed, is 175° in the **6a** isomer, where the Cl and vinyl groups occupy the axial positions, while it decreases to ca. 90° in the isomer **6b**, where a CO group replaces the Cl ligand in the axial position. From Figure 12 it can be noticed that conversion between **6a** and **6b** effectively takes place within 1.5 ps, as suggested by

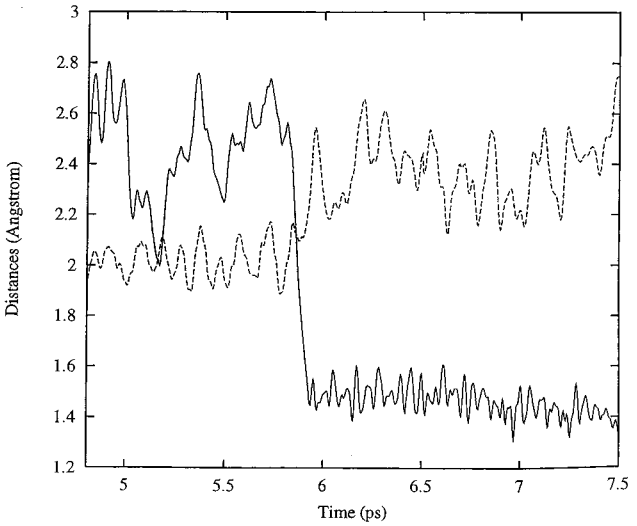

Figure 13. Time evolution of the C−C (carbonyl−vinyl) (solid line) and Ni−C (nickel−vinyl) (dashed line) distances for the second part of the dynamics simulation. Time in ps and distance in Å.

the fast decrease of the Cl−Ni−C angles observed between 1.0 and 1.5 ps; a similar decrease in this parameter is observed also around 0.5 ps and may be rationalized as an unsuccessful attempt of the conversion between the two isomers to take place. After 1.5 ps this parameter oscillates around 90°, close to its equilibrium value in **6b**. Figure 12 displays also the time evolution of the C−Ni−C (carbonyl−carbonyl) angle; this parameter is ca. 130° both in **6a** and **6b** and should therefore remain almost unchanged during the conversion between the two isomers. However, this parameter shows a decrease similar to that observed for the Cl−Ni−C angle within the same time span, suggesting that the exchange between axial and equatorial ligands takes place together with a crossing of two equatorial ligands and formation of a pyramidal intermediate.

Figure 13 displays the time evolution of the Ni−C (α carbon of the vinyl unit) distance together with the C−C distance (carbonyl−vinyl), for the time span going from 4.5 to 7.5 ps. Such a Ni−C distance is 1.96 Å both in the reagent **6a** and in the isomer **6b**, where the two atoms are bound, and 2.95 Å in the product **7**, where they are no longer bound. We can notice how the Ni−C distance follows almost a complementary trajectory with respect to the C−C distance; nevertheless this distance shows higher oscillations, after 6 ps, due to the fact that, at the end of the reaction, the Ni and C atoms are no longer bound.

The achievement of the CO migration is confirmed by the time evolution of C−Ni−C (carbonyl and vinyl carbons) angle in Figure 14, which shows a decrease from about 90° to about 30°, reflecting the approach of the carbonyl to the vinyl group. Figure 14 displays also the time evolution of the C−Ni−C (noninserting carbonyls) angle; this parameter is close to 100° both in complex **6b** and in the cis product **7a**, while a value close to 160° has been computed for the trans isomer **7b**. From Figure 14 it appears that this parameter increases steadily after 5.5 ps, in correspondence with the migrative CO insertion, while decreases again to a value close to 100° after ca. 1.2 ps, suggesting the initial product of the migrative insertion reaction is the trans isomer

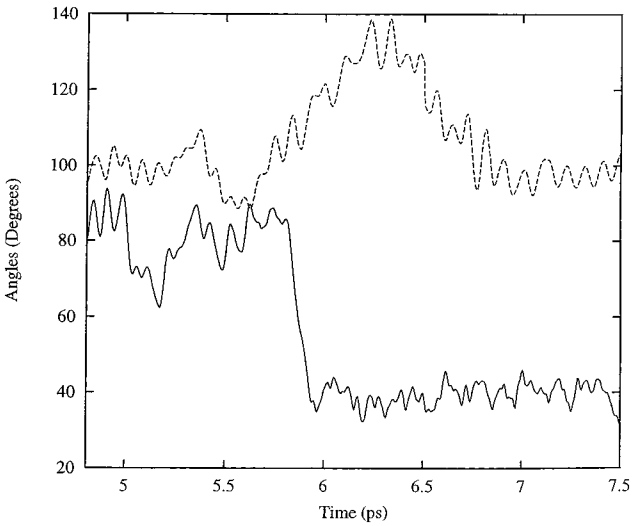

Figure 14. Time evolution of the C−Ni−C (carbonyl−vinyl) (solid line) and C−Ni−C (carbonyl−carbonyl) (dashed line) angles for the second part of the dynamics simulation. Time in ps and angles in deg.

of complex **7**, which suddenly relaxes to the more stable cis isomer.

Thus, we may conclude that the migrative insertion starting from **6a** proceeds via the formation of TBP isomer **6b** and occurs via a simultaneous detachment of the vinyl group from the metal and formation of the vinyl−carbonyl bond. Moreover we have observed that the initial product of the migrative insertion is the trans isomer **7b**, which relaxes to the more stable cis isomer within 1.2 ps.

3.3. Water Addition. The addition of a water molecule to **7** leads to the final elimination of the product, the acrylic acid CH_2═CHCOOH, and the regeneration the starting catalyst **2**. Due to the strongly acid conditions, this step probably occurs via the protonation of **7**, followed by the nucleophilic attack of a water molecule to the acyl carbon with the subsequent elimination of CH_2═CHCOOH; see Scheme 4.

Two protonated species can be conceived, corresponding to protonation at the acyl oxygen, **8**, or at the nickel atom, **9**. To gain further insight into the protonation mechanism of **7**, we performed a Mulliken charge and frontier orbital analysis of the latter complex, and the main results are collected in Tables 1 and 2. The calculated charges on acyl oxygen (−0.19) and nickel (+0.85) favor the formation of the O-protonated complex **8**. Table 2 also shows that the HOMO orbital (51 a), which is responsible for the nucleophilic character of **7**, is mainly localized on the nickel atom and the acyl oxygen with weights of, respectively, 35% and 17%. Frontier orbital factors seem, therefore, to favor Ni protonation. However, the electrophilic attack by a hard species such as the proton is usually a charge-dominated process, so that protonation on acyl oxygen is expected to be kinetically favored.

We then analyzed the relative thermodynamic stability and charge and frontier orbital distributions for **8** and **9**. We first computed the optimized geometries of the two protonated species for all the possible isomers without any symmetry constraints. For the tetracoordinated complex **8** the cis isomer was found significantly more stable than the trans isomer by 28 kJ mol^{-1}. For the pentacoordinated complex **9** the lowest isomer corresponds to a pyramidal geometry with the acyl

Table 1. Mulliken Charges on the Acyl Group, the α Vinyl Carbon, and the Metal for the Cis Isomers of 7 and 8, and for 9

	Q(Ni)	$Q(C_{acyl})$	$Q(O_{acyl})$	$Q(C_\alpha)$
7	0.85	−0.10	−0.19	−0.15
8	0.87	−0.20	−0.35	−0.14
9	0.86	0.08	−0.11	−0.20

Table 2. Energies and Composition of the Main Valence Orbitals for the Cis Isomer 7[a]

	occupied			unoccupied		
			HOMO	LUMO		
orbital	49 a	50 a	51 a	52 a	53 a	54 a
E (eV)	−6.55	−6.41	−5.92	−3.31	−3.17	−2.91
Ni	47.3	46.6	35.2	5.0	15.2	12.8
C_{acyl}	0.6	6.7	5.2	13.6	14.8	20.6
O_{acyl}	0.4	0.7	16.6	8.9	10.3	4.8
C_α	1.0	2.4	10.4	7.7	5.9	16.6

[a] Contributions from Ni, C_{acyl}, O_{acyl}, and C_α are reported.

Scheme 4

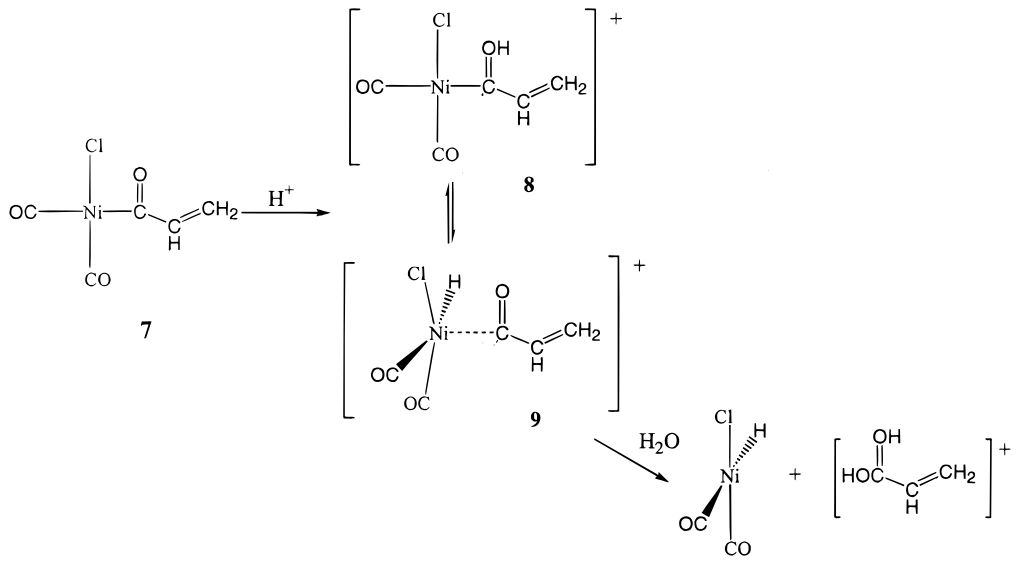

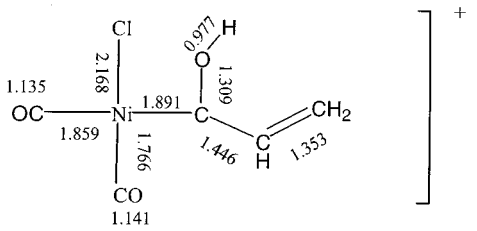

8

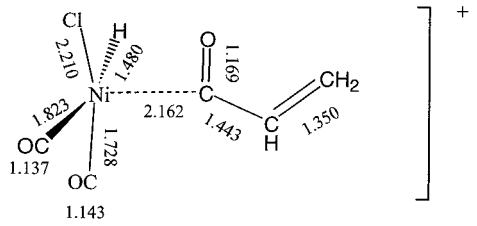

9

Figure 15. Main geometrical parameters of **8** and **9**. Distances in Å.

Table 3. Energies and Composition of the Main Valence Orbitals for the Cis Isomer 8[a]

	occupied			unoccupied		
			HOMO	LUMO		
orbital	49 a	50 a	51 a	52 a	53 a	54 a
E (eV)	−11.44	−11.37	−11.18	−8.27	−8.05	−7.64
Ni	35.3	36.8	71.5	22.5	10.3	4.9
C_{acyl}	4.3	1.0	2.7	21.5	35.0	13.1
O_{acyl}	.8	.3	1.4	6.0	6.1	3.8
C_α	4.6	3.2	2.6	2.3	1.9	17.5

[a] Contributions from Ni, C_{acyl}, O_{acyl}, are C_α are reported.

Table 4. Energy and Composition of the Main Valence Orbitals for 9[a]

	occupied			unoccupied		
			HOMO	LUMO		
orbital	49 a	50 a	51 a	52 a	53 a	54 a
E (eV)	−11.54	−11.23	−10.81	−7.92	−7.67	−7.15
Ni	82.8	75.8	94.9	0.1	28.3	8.6
C_{acyl}	0.1	0.1	.6	27.7	0.1	0.1
O_{acyl}	0.1	0.2	1.0	0.4	8.9	26.8
C_α	0.1	0.1	1.0	0.4	8.9	26.8

[a] Contributions from Ni, C_{acyl}, O_{acyl}, and C_α are reported.

group in apical position. The optimized structures are reported in Figure 15.

The O-protonated complex was found to be more stable than the Ni-protonated by 35 kJ mol^{-1}. However, due to this low energy difference, **8** and **9** could easily interconvert at the reaction temperature (500 K), giving rise to a tautomeric equilibrium.

An analysis of the Mulliken charges (Table 1) and frontier orbital distribution of **8** and **9** (Tables 3 and 4) shows that the nucleophilic attack of water on the acyl carbon is easier for **9** than for **8**. Indeed the charge on the acyl carbon is higher in **9** (+0.08) than in **8** (−0.20), and the LUMO is localized mainly on the acyl carbon in **9**, with a high out-of-plane p_z character, while it is more uniformly distributed on nickel and on the acyl carbon in **8**.

Moreover, a better analysis of the optimized geometry for **9** shows a quite long Ni−C(acyl) bond length, 2.162 Å, ca. 0.2 Å longer than in the tetracoordinated acyl complexes **4** (1.916 Å) and **7** (1.979 Å), and a quasi-planar coordination around the nickel by the remaining ligands, with a geometry very close to that of **2**. This means that the Ni−C(acyl) bond is weakened by the protonation at the Ni atom, so that the detachment of the COCH=CH_2 group should occur quite easily upon attack of the water molecule to the acyl carbon, leading to the easy elimination of protonated propenoic acid.

Step d of the catalytic cycle may therefore be considered as constituted by two elementary paths: (i) the protonation of **7**, to give either the O-protonated complex **8** or the Ni-protonated isomer **9**, eventually related by a tautomeric equilibrium, (ii) the attack of a water molecule to the partially positively charged carbonyl α carbon followed by the final elimination of CH_2=CHCOOH and the regeneration of the starting catalyst **2**; see Scheme 4.

The overall reaction step,

$$Cl(CO)_2NiHCOCH{=}CH_2 + H_2O \rightarrow Cl(CO)_2NiH + CH_2{=}CHCOOH$$

was found sightly exothermic by 12 kJ mol^{-1}.

Actually, the corresponding step among protonated species,

$$Cl(CO)_2HNi{-}CO{-}CH{=}CH_2^+ + H_2O \rightarrow Cl(CO)_2NiH + CH_2{=}CHCOOH_2^+$$

which is the one actually occurring in the experimental conditions, was found more exothermic, 40 kJ mol^{-1}.

The computed value for the exothermicity of the overall catalytic cycle is −290 kJ mol^{-1}. The value of ΔH at 298 K for the reaction CO + H_2O + H_2C_2 → CH=CH_2COOH, computed from the formation enthalpies of the involved molecules (NIST webbook, http://webbook.nist.gov), is −211.3 kJ mol^{-1}. Such a large discrepancy cannot be attributed to the neglect of zero-point vibrations and thermal effects. A possible reason for this discrepancy could be the basis set superposition error (BSSE). Indeed, the formation of acrylic acid involves the fusion of three small molecules and BSSE effects might be quite important. To clarify this point, we have estimated the BSSE for the overall reaction by extrapolating the energy difference computed at our level of theory to that corresponding to an infinite basis set expansion, for which BSSE is zero, according to the method proposed by Martin.[27] The BSSE correction was computed to be 51 kJ mol^{-1}, such that the corrected value for the ΔE of the overall reaction is now −239 kJ mol^{-1}, which is reasonably close to the value of the ΔH at 298 K, considering that we are neglecting thermal contributions to the total energy. The residual calculations presented in this paper should be less affected by BSSE, due to the fact that many of them are intramolecular rearrangements or involve the addition of only a small molecule to a large fragment.

3.4. Energy Profile of the Full Catalytic Cycle. By combining the energies of the intermediates and

(27) Martin, J. M. L. *Chem. Phys. Lett.* **1996**, *259*, 669.

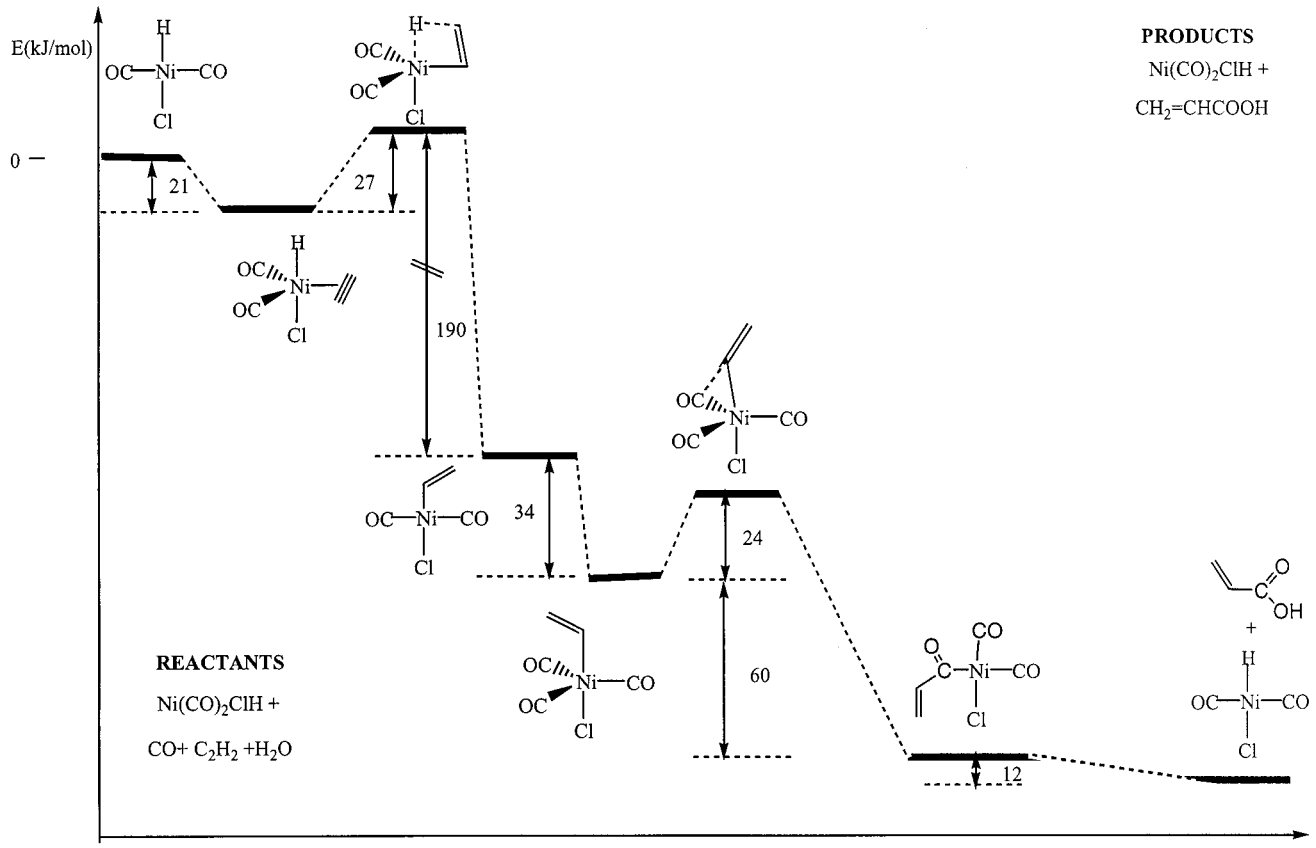

Figure 16. Schematic representation of the potential energy surface for the whole catalytic cycle of the carbonylation of acetylene. Only lower energy pathways are reported. Energies in kJ mol^{-1}.

Table 5. Summary of the Energy Differences (ΔE) and Activation Barriers E_a, in kJ mol^{-1}, for All the Considered Reactions[a]

step	reaction	ΔE	E_a
a	$Ni(CO)_4 + HCl \rightarrow Cl(CO)_2NiH + 2CO$	213	
	$Cl(CO)_2NiH + HC{\equiv}CH \rightarrow Cl(CO)_2NiH(HC{\equiv}CH)$	−21[a]	
		−5[b]	
b			
	$Cl(CO)_2NiH(HC{\equiv}CH) \rightarrow Cl(CO)_2Ni{-}CH{=}CH_2$	−168[a]	27[a]
		−184[b]	15[b]
c′	$Cl(CO)_2Ni{-}CH{=}CH_2 \rightarrow Cl(CO)Ni{-}CO{-}CH{=}CH_2$	−16	9
	$Cl(CO)Ni{-}CO{-}CH{=}CH_2 + CO \rightarrow Cl(CO)_2Ni{-}CO{-}CH{=}CH_2$	−80	
	$Cl(CO)_2Ni{-}CH{=}CH_2 + CO \rightarrow Cl(CO)_3Ni{-}CH{=}CH_2$	−34[a]	
c″		−26[b]	
	$Cl(CO)_3Ni{-}CH{=}CH_2 \rightarrow Cl(CO)_2Ni{-}CO{-}CH{=}CH_2$	−60[a]	24[a]
		−68[b]	17[b]
d	$Cl(CO)_2NiHCO{-}CH{=}CH_2^+ + H_2O \rightarrow Cl(CO)_2NiH + CH_2{=}CHCOOH^+$	−40	

[a,b] Refer to the two lowest TBP isomers involved in steps *b*, *c′*, and *c″*.

transition states for all the elementary reactions discussed above, we built the energy profile for the full catalytic cycle reported in Figure 16, while a detailed summary of the energetics of all the considered reactions may be found in Table 5. For the intermediates involving more than one isomer we considered only the most stable one, and for step d we considered the reaction between the protonated species. As seen from the Figure 16, all the steps involved in the catalytic cycle are exothermic, and the final products lie energetically −290 kJ mol^{-1} below the reactants (−239 kJ/mol, when accounting for BSSE correction).

Moreover, all the steps present low or negligible energy barriers, the highest one being 27 kJ mol^{-1}, and the activation barrier for the overall reaction is only 6 kJ mol^{-1}.

However, the preliminary generation of the active catalyst **2**,

$$Ni(CO)_4 + HCl \rightarrow Cl(CO)_2NiH + 2CO$$

is highly endothermic (213 kJ mol^{-1}). The catalyzed carbonylation of acetylene is therefore a thermodynamically favored and kinetically easy process, and quite drastic reaction conditions are probably required to form an appreciable concentration of the active catalyst.

4. Conclusions

Static and dynamic density functional calculations have been performed on nearly all the intermediates involved in each step of the catalytic cycle for the Reppe

carbonylation of acetylene. The main purpose of the present investigation was to evaluate the overall thermodynamics and kinetics for the full catalytic cycle and to rationalize the reaction dynamics for some of the main steps of the cycle.

The insertion reaction of acetylene into the Ni−H bond was found highly exothermic (−189 kJ mol^{-1}) with a small activation barrier of 27 kJ mol^{-1}.

The CO insertion into the Ni−vinyl bond has also been found quite exothermic (−94 kJ mol^{-1}, including the coordination by a further CO molecule), and with a small energy barrier. Moreover, dynamic simulations performed on $Cl(CO)_3Ni-CH=CH_2$ show that the migrative insertion begins from the **6b** isomer and occurs via a simultaneous detachment of the vinyl group from the metal and formation of the vinyl−carbonyl bond.

We built the overall energy profile for the full catalytic cycle and found that the Reppe carbonylation of acetylene is a thermodynamically favored and kinetically easy process, and quite drastic reaction conditions are probably required to form an appreciable concentration of the active catalyst.

Acknowledgment. We acknowledge the CNR and the MURST for financial support.

OM0002428